An Analysis of Vibrating Euler-Bernoulli Beams

using Finite Element, Newmark and Eigenvalue Methods

Dylan Everingham, Sebastian Myrbäck, Sergi Andreu,
Carsten van de Kamp

September 2021

Technische Universität Berlin

Contents

1 Introduction

In modern mechanical engineering, understanding vibrations or deformations in complex structures is crucial for developing robust and working devices. Often, a trial-and-error approach is economically unfeasible and therefore one should resort to modelling the to-be-developed device on a computer, think of researching how to control and stabilise flexible systems, such as robot arms or spacecraft with flexible appendages [1].

One can also think of rotating beams, such as a helicopters with rotor blades. A new mechanical difficulty arises here, since there is a coupling between elastic deformations and rigid-body motions. This is considered in for example [2, 3]. Again, numerical simulations are a crucial part of devising or improving appliances.

However, also in non-engineering sciences, such as nanobiology, the understanding of the mechanical properties of beams has become more important in recent years. Consider for example microtubules. These are beam-shaped proteins, organized in a network, forming the most rigid and complex part of the cytoskeleton of a living cell. Their properties play an important role in many biological processes, such as cell division and intracellular transport [4]. Their bending properties can be modelled as an Euler-Bernoulli beam [5].

This text will focus on applying different methods of numerical analysis to the Euler-Bernoulli beam theory, revealing multiple ways or starting points for a specific beam-related research. In chapter two, we will familiarise the reader with the Euler-Bernoulli beam by presenting a derivation of the governing equations and the underlying assumptions. Moreover, we will consider the different analytical and numerical methods that are applied in this work. Subsequently, in chapter three, we present the outcomes of the numerical analysis of beams under various conditions and compare the results with analytical solutions for simple cases. Here, we both consider static beam deformations, as well as dynamically vibrating beams. Ultimately, we present the conclusions in combination with recommendations for further research in chapter four.

This work is part of the course Project Numerical Analysis in the master's programme Computer Simulations for Science and Engineering (COSSE), conducted at the faculty of Mathematics and Natural Sciences at the Technische Universität Berlin.

2 Theory

2.1 The Euler-Bernoulli beam equation

First, we will present a derivation of the Euler-Bernoulli beam equation that is studied in this work. The derivation is based on [6]. There, one can also find a more detailed discussion.

Consider an elastic beam, such that the x–axis coincides with its natural axis when no forces are applied. Let $u_x(x, z, t)$ and $u_z(x, z, t)$ be respectively the axial and transverse displacements of the material particle, and $u(x, t)$, $w(x, t)$ the corresponding displacement of the material particles with respect to the beam in the rest configuration, corresponding to $z = 0$.

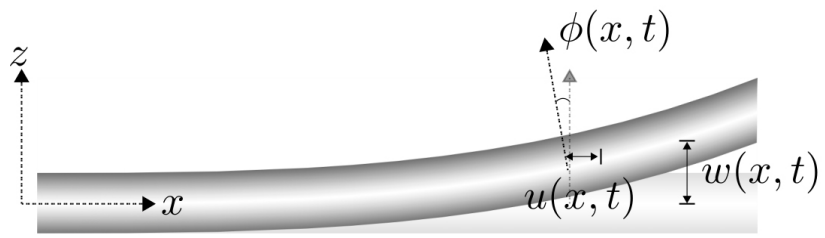

Figure 2.1: Diagram and parameters of the elastic beam.

Then the Kirchhoff kinematic equations state that

$$u_x(x, z, t) = u(x, t) - z\phi(x, t), \tag{2.1}$$

$$u_z(x, z, t) \cong w(x, t), \tag{2.2}$$

where $\phi(x, t)$ is the rotation of the cross section of the beam, originally located at the coordinate x.

We define the infinitesimal axial strain as

$$\epsilon_{xx}(x, z, t) = \frac{\partial u_x}{\partial x} \tag{2.3}$$

and

$$\epsilon(x, t) = \frac{\partial u}{\partial x}. \tag{2.4}$$

By substituting (2.1) in (2.3) we get the strain distribution, given by

$$\epsilon_{xx}(x, z, t) = \epsilon(x, t) - z\kappa(x, t), \tag{2.5}$$

where κ represents the curvature of the neutral axis of the beam originally located at the coordinate x, and it is given by

$$\kappa(x, t) = \frac{\partial \phi}{\partial x}. \tag{2.6}$$

Under small stress, we can consider the beam to behave locally as a spring. The axial stress $\sigma_{xx} = \sigma(x, z, t)$ is then related to the strain by Hooke's law,

$$\sigma(x, z, t) = E(x)\epsilon_{xx}(x, z, t), \tag{2.7}$$

where σ is the axial stress, ϵ_{xx} is the infinitesimal axial strain, and E is the young modulus of the beam. The axial force $N(x, t)$ is calculated by integrating over the area of cross section at x,

$$N(x, t) = \int_A \sigma(x, z, t) dA. \tag{2.8}$$

Combining the previous equations yields

$$N(x, t) = \int_A E(x)\epsilon_{xx}(x, z, t) dA = E(x)\epsilon(x, t) \int_A dA - E(x)\kappa(x, t) \int_A z dA. \tag{2.9}$$

Now, since $z = 0$ at the area centroid, we have

$$\int_{A(x)} z dA = 0, \tag{2.10}$$

and thus

$$N(x, t) = E(x)A\epsilon(x, t) = E(x)A\frac{\partial u}{\partial x}. \tag{2.11}$$

In a similar manner, we can get an equation for the moment $M(x, t)$, defined as

$$M(x, t) = \int_A \sigma(x, z, t) z dA, \tag{2.12}$$

where we have

$$M(x, t) = E(x)\epsilon(x, t) \int_A z dA - E(x)\kappa(x, t) \int_A z^2 dA. \tag{2.13}$$

Using equation 2.10, we find

$$M(x,t) = -E(x)I\kappa(x,t), \tag{2.14}$$

where $I = I(x) = \int_{A(x)} z^2 dA$ is the moment of inertia.

The shear force $Q(x,t)$ is given by

$$Q(x,t) = \int_{A(x)} \tau(x,z,t) dA, \tag{2.15}$$

where $\tau(x,z,t)$ is the transverse shear stress acting on that cross section. Using Newton's Second Law in the transverse direction, we find

$$q(x,t)dx + \left[Q(x,t) + \frac{\partial Q}{\partial x}dx\right] - Q(x,t) = \mu(x)dx\frac{\partial^2 w}{\partial t^2}, \tag{2.16}$$

which reduces to

$$q(x,t) + \frac{\partial Q}{\partial x} = \mu(x)\frac{\partial^2 w}{\partial t^2}. \tag{2.17}$$

Considering the local density moment $b(x,t)$, we have that

$$\begin{aligned} b(x,t)dx - \left[M(x,t) + \frac{\partial M}{\partial x}dx\right] + M(x,t) \\ + \left[Q(x,t) + \frac{\partial Q}{\partial x}dx\right]\frac{dx}{2} + Q(x,t)\frac{dx}{2} = I_p(x)dx\frac{\partial^2 \phi}{\partial t^2}. \end{aligned} \tag{2.18}$$

Neglecting terms of order $\mathcal{O}(dx)^2$,

$$Q(x,t) = \frac{\partial M}{\partial x} + I_p(x)\frac{\partial^2 \phi}{\partial t^2} - b(x,t), \tag{2.19}$$

where $I_\rho(x) = \mu(x)I(x)$ is the rotatory inertia of the beam.

Using the above equations, one arrives at

$$q(x,t) - \frac{\partial b}{\partial x} - \frac{\partial^2}{\partial x^2}EI\frac{\partial \phi}{\partial x} = \mu(x)\frac{\partial^2 w}{\partial t^2} - \frac{\partial}{\partial x}I_p\frac{\partial^2 \phi}{\partial t^2}, \tag{2.20}$$

which can be considered as a general beam equation.

Now, under the assumption that we have small and smooth deflections, we can consider $\phi(x,t) \cong \frac{\partial w}{\partial x}$, and thus

$$\kappa(x,t) = \frac{\partial \phi}{\partial x} \cong \frac{\partial^2 w}{\partial x^2}, \tag{2.21}$$

$$M(x,t) = -EI\kappa(x,t) \cong -EI\frac{\partial^2 w}{\partial x^2}, \tag{2.22}$$

$$\frac{\partial^2 \phi}{\partial t^2} \cong \frac{\partial^2}{\partial t^2}\frac{\partial w}{\partial x} = \frac{\partial}{\partial x}\frac{\partial^2 w}{\partial t^2}. \tag{2.23}$$

Substituting these relations into equation 2.20 and setting $I_p = 0$ we get

$$\mu(x)\frac{\partial^2 w}{\partial t^2} + \frac{\partial^2}{\partial x^2}E(x)I(x)\frac{\partial^2}{\partial x^2}w = q(x,t) - \frac{\partial b}{\partial x}. \tag{2.24}$$

Considering $E(x)I(x) = EI$ constant through the beam, this equation reduces to

$$\mu(x)\frac{\partial^2 w}{\partial t^2} + EI\frac{\partial^4 w}{\partial x^4} = q(x,t) - \frac{\partial b}{\partial x}. \tag{2.25}$$

We treat the mass distribution as being concentrated along the axis of the beam, which is a reasonable approximation, and hence we neglect the rotatory inertia of the beams, thus setting $\frac{\partial b}{\partial x} = 0$.

$$\mu\frac{\partial^2 w}{\partial t^2} + EI\frac{\partial^4 w}{\partial x^4} = q. \tag{2.26}$$

This is the Euler-Bernoulli beam equation. In the following, we consider this equation on the set of piecewise twice differentiable functions $V := C^{2,p}(0,L)$. That is, $q \in V$ and $EI\frac{\partial^2 w}{\partial x^2} \in V$.

2.2 Analytical solutions

In the problem setting of this report, we consider a one dimensional model of a beam with domain $\Omega = [0,L]$ for a given length $L \in \mathbb{R}^+$ such that $w(x)$ is the function describing the bending curve at each point $x \in [0,L]$, under the assumption that $EIw'' \in V$. As above, $q(x)$ denotes the load (force density) at x under the assumption that $q \in V$. For physical intuition, we use the notation $M^x(w) = EIw''(x)$ which denotes the bending moment of the beam at x, and $Q^x(w) = -(EIw'')'(x)$ which denotes the shear force at x, in accordance with the previous section.

In this section, we derive analytical solutions to the Euler-Bernoulli beam equation (2.26) in the static case and for constant flexural rigidity EI, in which the equation reduces to

$$EI\frac{\partial^4 w}{\partial x^4} = q. \tag{2.27}$$

For an integrable function $f : [a,b] \longrightarrow \mathbb{R}$, we denote its primitive function $f^{[1]}$, its second primitive function $f^{[2]} = (f^{[1]})^{[1]}$ (if it exists), and similarly for higher orders, borrowing the

notation from [7]. Additionally, we assume that any primitive function of the load q will be zero at $x = 0$. Finally, under the assumptions that EI is non-zero (which is physically obvious), and that the fourth primitive function of q exists, the general solution of (2.27) can be written as

$$w = \frac{q^{[4]}}{EI} + C_0 + C_1 x + C_2 x^2 + C_3 x^3, \tag{2.28}$$

where $C_i \in \mathbb{R}$ for $i = 0, 1, 2, 3$. Taking the derivatives of this solution yields

$$w'(x) = \frac{q^{[3]}}{EI} + C_1 + 2C_2 x + 3C_3 x^2 \tag{2.29}$$

$$w''(x) = \frac{q^{[2]}}{EI} + 2C_2 + 6C_3 x \tag{2.30}$$

$$w'''(x) = \frac{q^{[1]}}{EI} + 6C_3. \tag{2.31}$$

Four unknown coefficients require four different equations to give a unique solution, and this is therefore the amount of boundary conditions that we require for our problem. The boundary conditions together with the equations (2.28)–(2.31) will provide the unique solution. Moreover, the boundary conditions will, of course, depend on the type of beam problem we are solving and we will therefore treat these different cases separately below.

2.2.1 Cantilever beam

The first case that we treat in this report is the bending of a beam clamped at its left side and free at the other, whereby the following boundary conditions hold

$$w(0) = a, \qquad w'(0) = b, \qquad Q^L(w) = Q_L, \qquad M^L(w) = M_L, \tag{2.32}$$

where the constants $a, b, Q_L, M_L \in \mathbb{R}$ are given numbers. Using the fact that $Q^L(w) = -EIw'''(L)$ and $M^L(w) = EIw''(L)$, we can insert the boundary conditions (2.32) in the equations (2.28)–(2.31), resulting in the following equations

$$\begin{aligned} w(0) &= C_0 = a \\ w'(0) &= C_1 = b \\ w''(L) &= \frac{q^{[2]}(L)}{EI} + 2C_2 + 6C_3 L = \frac{M_L}{EI} \\ w'''(L) &= \frac{q^{[1]}(L)}{EI} + 6C_3 = -\frac{Q_L}{EI}. \end{aligned}$$

From these equations, we obtain the coefficients $C_0 = a$, $C_1 = b$, $C_2 = (Q_L L + M_L + q^{[1]}(L)L - q^{[2]}(L))/2EI$ and $C_3 = -(Q_L + q^{[1]}(L))/6EI$ and the corresponding solution to (2.27) as

$$w(x) = \frac{q^{[4]}(x)}{EI} + a + bx + \frac{Q_L L + M_L + q^{[1]}(L)L - q^{[2]}(L)}{2EI} x^2 - \frac{Q_L + q^{[1]}(L)}{6EI} x^3.$$

In the simulations performed in this report, we examined the physical parameters q, a, b, Q_L and M_L individually, keeping one non-zero and the rest to zero. The following three cases were examined

1. **Load at free end:** For non-zero Q_L and $q = a = b = M_L = 0$, the analytical solution reduces to

$$w(x) = \frac{Q_L}{6EI}(3Lx^2 - x^3). \tag{2.33}$$

2. **Moment at free end:** For non-zero M_L and $q = a = b = Q_L = 0$, the analytical solution reduces to

$$w(x) = \frac{M_L x^2}{2EI}. \tag{2.34}$$

3. **Constant load density:** For a non-zero constant $q = q_0$ and $a = b = Q_L = M_L = 0$, the analytical solution reduces to

$$w(x) = \frac{q_0}{24EI}(x^4 - 4Lx^3 + 6L^2x^2). \tag{2.35}$$

The simulations of these three cases are illustrated in the **Results and discussion** chapter.

2.2.2 Supported beam at both ends

The second case that was investigated consists of a beam supported at both ends, uniquely determined by the boundary conditions

$$w(0) = a_0, \qquad w(L) = a_L, \qquad M^0(w) = M_0, \qquad M^L(w) = M_L. \tag{2.36}$$

Inserting the boundary conditions from (2.36) in (2.28) and (2.30) yields

$$\begin{aligned} w(0) &= C_0 = a_0 \\ w(L) &= \frac{q^{[4]}(L)}{EI} + C_0 + C_1 L + C_2 L^2 + C_3 L^3 = a_L \\ w''(0) &= 2C_2 = \frac{M_0}{EI} \\ w''(L) &= \frac{q^{[2]}(L)}{EI} + 2C_2 + 6C_3 L = \frac{M_L}{EI}. \end{aligned}$$

Solving this linear system, the solution is given by

$$w(x) = \frac{q^{[4]}}{EI} + a_0 + \left(\frac{a_L - a_0}{L} x - \frac{L}{6EI}(2M_0 + M_L - q^{[2]}(L)) - \frac{q^{[4]}(L)}{EIL} \right) x + \frac{M_0}{2EI} x^2 + \frac{1}{6EIL}(M_L - M_0 - q^{[2]}(L))x^3.$$

In the supported case, the following cases were simulated

1. **Moment at ends:** For a number $M \in \mathbb{R}$, we let $M_0 = M$ and $M_L = -M$. With $a_0 = a_L = q = 0$, the analytical solution reduces to

$$w(x) = -\frac{M}{EI}\left(\frac{x^3}{6L} - \frac{x^2}{2} + \frac{Lx}{6}\right). \tag{2.37}$$

2. **Constant load density:** For a number $q_0 \in \mathbb{R}$, $q(x) = q_0$ and $M_0 = M_L = a_0 = a_L = 0$, the analytical solution reduces to

$$w(x) = \frac{q_0}{24EI}x^4 - \frac{q_0 L}{12EI}x^3 + \frac{q_0 L^3}{24EI}x. \tag{2.38}$$

3. **Load and moment:** For the last case, a combination of 1. and 2. was simulated, and hence the full solution analytical solution is given by

$$w(x) = \frac{q_0}{24EI}x^4 - \frac{1}{6EI}(2ML + q_0 L/2)x^3 + \frac{M}{2EI}x^2 + \frac{1}{EI}(q_0 L^3/24 - ML/6)x. \tag{2.39}$$

As in the cantilever beam case, the simulations are illustrated in the chapter **Results and discussion**.

The two models – the cantilever and the two-side supported beam – are visualized in Figure 2.2.

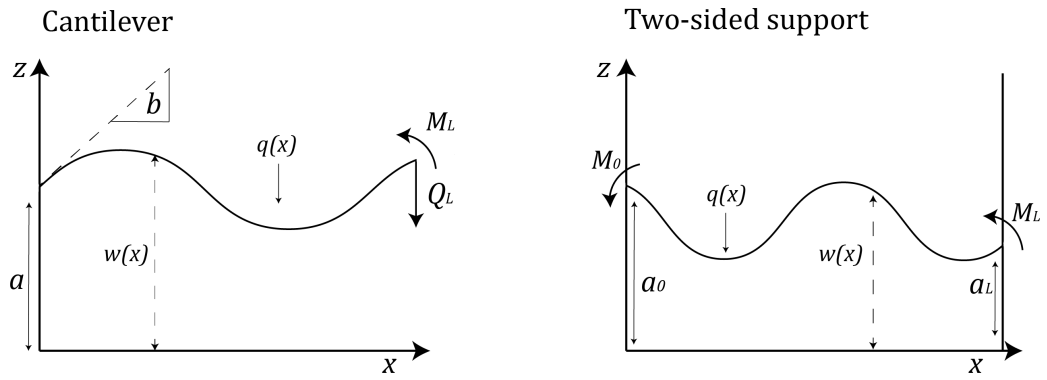

Figure 2.2: Schematic of the relavant quantities and boundary conditions corresponding to the cantilever case (left) and the two-sided support case (right).

2.3 Analytical solutions: Eigenvalue method

In the case that there are no external forces and moments and we have homogeneous boundary conditions, the dynamic beam equation 2.26 can be analytically solved with the eigenvalue method. This method is extensively described in [8]. In this work, we only use some results in

order to compare simple numeric solutions to the dynamic beam equation. These results will be summarized next.

The eigenvalue method solution to the dynamic beam equation consists of a time- and a space-dependent part. For both the cantilever beam, as the beam with support at both ends, the solution is given as

$$w(x,t) = \sum_{j=1}^{\infty} \left[\left\langle w_j, w(x,0) \right\rangle \cos(\omega_j t) + \frac{\left\langle w_j, \dot{w}(x,0) \right\rangle}{\omega_j} \sin(\omega_j t) \right] w_j(x), \tag{2.40}$$

with initial conditions $w(x,0)$ and $\dot{w}(x,0)$. w_j represents the j-th eigenfunction, as described in [8]. These eigenfunctions are different in the cantilever and the both side supported case.

The eigenfrequencies ω_j for $j \in \mathbb{N}$ are given as

$$\omega_j = \sqrt{\frac{EI}{\mu}} \kappa_j^2, \tag{2.41}$$

for constant $E, I, \mu > 0$. For the cantilever beam, we have $\kappa_j \approx \frac{(j-1/2)\pi}{L}$ and for the beam supported at both ends, we find $\kappa_j \approx \frac{j\pi}{L}$.

2.4 Finite Element Method

In order to numerically solve the Euler-Bernoulli beam equation 2.26, we will consider the Finite Element Method (FEM). The following results are described by [7].

First, we consider the weak formulation of the dynamic beam equation 2.26. Let $\psi = \psi(x) \in V$, then multiplying equation 2.26 by ψ, integrating over the domain $[0, L]$ and applying partial integration, we find

$$\int_0^L \mu \ddot{w}(x,t)\psi \, dx + \int_0^L EI w''(x,t)\psi'' \, dx = \int_0^L q(x,t)\psi \, dx + b(\psi, t), \tag{2.42}$$

where

$$b(\psi, t) = Q_L(t)\psi(L) - Q_0(t)\psi(0) + M_L(t)\psi'(L) - M_0(t)\psi'(0). \tag{2.43}$$

This holds for any $\psi \in V$, in particular for any $\phi_i \in V_h \subset V, i \in \{1, ..., n\}$, where V_h is an finite, n-dimensional Ansatzspace with basis $\phi_1, ..., \phi_n : [0, L] \longrightarrow \mathbb{R}$.

Now let

$$w_h(x,t) = \sum_{k=1}^{N} w_k(t)\phi_k(x) \tag{2.44}$$

be the projection of the FEM solution onto V_h, where $w_k(t) : [t_0, t_e] \longrightarrow \mathbb{R}$ is the time dependent coefficient for the basis function ϕ_k for $k = 1, ..., N$. Then testing the weak formulation for

$\phi_j \in V_h$ yields

$$\begin{aligned}\int_0^L \mu \ddot{w}_h(x,t)\phi_j \, dx + \int_0^L EI w_h''(x,t)\phi_j'' \, dx \\ &= \sum_{k=1}^{N} \left(\int_0^L \mu \phi_k \phi_j \, dx \right) \ddot{w}_k(t) + \sum_{k=1}^{N} \left(\int_0^L EI \phi_k'' \phi_j'' \, dx \right) w_k(t) \\ &= \int_0^L q(t)\phi_j \, dx + Q_L(t)\phi_j(L) - Q_0(t)\phi_j(0) + M_L(t)\phi_j'(L) - M_0(t)\phi_j'(0).\end{aligned}$$

The equations for all $j = 1, ...N$ can be written together in matrix form as

$$M\ddot{w}(t) + Sw(t) = q(t) + Q_L(t)e_L - Q_0(t)e_0 + M_L(t)d_L - M_0(t)d_0, \tag{2.45}$$

where

$$\begin{aligned} w(t) &= \begin{bmatrix} w_1(t) & w_2(t) & \dots & w_N(t) \end{bmatrix}^\mathsf{T}, \\ q(t) &= \begin{bmatrix} \int_0^L q(t)\phi_1 \, dx & \int_0^L q(t)\phi_2 \, dx & \dots & \int_0^L q(t)\phi_N \, dx \end{bmatrix}^\mathsf{T}, \\ e_x &= \begin{bmatrix} \phi_1(x) & \phi_2(x) & \dots & \phi_3(x) \end{bmatrix}^\mathsf{T}, \\ d_x &= \begin{bmatrix} \phi_1'(x) & \phi_2'(x) & \dots & \phi_3'(x) \end{bmatrix}^\mathsf{T}. \end{aligned}$$

$S \in \mathbb{R}^{N,N}$ denotes the symmetric and positive definite stiffness matrix, defined as

$$S = \begin{bmatrix} s_{i,j} \end{bmatrix}_{i,j=1,\dots,N} = \left[\int_0^L EI \phi_i'' \phi_j'' \, dx \right]_{i,j=1,\dots,N},$$

and $M \in \mathbb{R}^{N,N}$ represents the symmetric and positive definite mass matrix, defined as

$$M = \begin{bmatrix} m_{i,j} \end{bmatrix}_{i,j=1,\dots,N} = \left[\int_0^L \mu \phi_i \phi_j \, dx \right]_{i,j=1,\dots,N}.$$

For the cantilever beam, we add two Dirichlet boundary conditions

$$\begin{aligned} w_h(0,t) &= a \\ w_h'(0,t) &= b, \end{aligned}$$

just as before. This allows us to write the extended system as

$$\begin{bmatrix} M & 0 & 0 \\ 0 & 0 & 0 \\ 0 & 0 & 0 \end{bmatrix} \begin{bmatrix} \ddot{w}(t) \\ \ddot{Q}_0(t) \\ \ddot{M}_0(t) \end{bmatrix} + \begin{bmatrix} S & e_0 & d_0 \\ e_0^\mathsf{T} & 0 & 0 \\ d_0^\mathsf{T} & 0 & 0 \end{bmatrix} \begin{bmatrix} w(t) \\ Q_0(t) \\ M_0(t) \end{bmatrix} = \begin{bmatrix} q(t) + Q_L(t)e_L + M_L(t)d_L \\ a \\ b \end{bmatrix}, \tag{2.46}$$

where we will refer to the first and second matrix on the left-hand side as the extended mass matrix M_e and the extended stiffness matrix S_e respectively.

In the case the beam is supported at both ends, we add the Dirichlet boundary conditions

$$\begin{aligned} w_h(0,t) &= a_0 \\ w_h(L,t) &= a_L, \end{aligned}$$

such that the extended system becomes

$$\begin{bmatrix} M & 0 & 0 \\ 0 & 0 & 0 \\ 0 & 0 & 0 \end{bmatrix} \begin{bmatrix} \ddot{w}(t) \\ \ddot{Q}_0(t) \\ \ddot{Q}_L(t) \end{bmatrix} + \begin{bmatrix} S & e_0 & -e_L \\ e_0^\mathsf{T} & 0 & 0 \\ -e_L^\mathsf{T} & 0 & 0 \end{bmatrix} \begin{bmatrix} w(t) \\ Q_0(t) \\ Q_L(t) \end{bmatrix} = \begin{bmatrix} q(t) - M_0(t)d_0 + M_L(t)d_L \\ a_0 \\ -a_L \end{bmatrix}. \tag{2.47}$$

In order to be able to solve these systems, it remains to define the grid and the Ansatzspace V_h. We discretize the interval $[0, L]$ with a uniform grid, defined by the nodes $x_i = h(i-1)$ for $i = 1, ..., n$ and grid spacing $h = \frac{L}{n-1}$. Now, we take V_h as the space of piecewise cubic polynomials on the grid $\{x_i : i = 1, ..., n\}$, i.e.

$$V_h = \{\phi \in V : \phi|_{(x_i, x_{i+1})} \text{ is a polynomial of degree } d \leq 3, i = 1, ..., n-1\}.$$

The basis functions for V_h can be taken from the following form functions

$$\begin{aligned} \bar{\phi}_1(\xi) &= 1 - 3\xi^2 + 2\xi^3, \\ \bar{\phi}_2(\xi) &= \xi(\xi - 1)^2, \\ \bar{\phi}_3(\xi) &= 3\xi^2 - 2\xi^3, \\ \bar{\phi}_4(\xi) &= \xi^2(\xi - 1), \end{aligned}$$

by rescaling them on each grid element, as described in [7]. Note, that $\bar{\phi}_1$ and $\bar{\phi}_3$ are defined such that they take the value 1 at the left, respectively, right nodes of the element they are defined on. The form functions $\bar{\phi}_2$ and $\bar{\phi}_3$ attain value 0 on the nodes, but attain a slope of 1 in the left and right nodes of the element they are defined on. This makes it possible to control both the value and the derivative in the node points of any linear combination of functions from V_h. Note that we also need this in order to solve this fourth order PDE.

In addition, we remark that for the Ansatzspace V_h the Galerkin appoximation of the solution $w_h(x, t)$ coincides with the exact solution $w(x, t)$ in the nodes of the grid.

In order to numerically solve the static beam equation 2.27, we can simply set $\ddot{w}(t) = 0$ and define all time-dependent boundary conditions as constants. This results in a sparse system of linear equations, which can be solved by a sparse solver. The Python implementation, using local mass- and stiffness matrices and backtracing transformations to the reference element $[0, 1]$ is attached to this report, as part of attachment A.

In order to numerically solve the *dynamic* beam equation, we will consider two different methods in the next two sections.

2.5 The dynamic beam equation: Newmark method

The first method with which we can numerically solve the dynamic equation 2.26, is the Newmark Method [9]. It has the advantage of solving second-order equations directly, instead of transforming the equation to a pair of simultaneous first-order differential equations, and then solving with first-order methods such as Runge-Kutta.

Denoting $u : [t_1, t_e] \longrightarrow \mathbb{R}^n$ the solution of the equation

$$f(\ddot{u}(t), \dot{u}(t), u(t), t) = 0, \tag{2.48}$$

we want to find solutions $(\ddot{u}_i, \dot{u}_i, u_i, t_i)$ at the discrete time filtration given by $t_1 < t_i < t_e$ such that the initial conditions are guaranteed, $u_1 = u(t_1)$, $\dot{u}_1 = \dot{u}(t_1)$, $\ddot{u}_1 = \ddot{u}(t_1)$, and that obey the equation 2.48, that is $f(\ddot{u}_i, \dot{u}_i, u, t) = 0$ for $i = 2, ..., n$.

Using Taylor expansions, we arrive at the iterated system

$$u_{j+1} = u_j^* + \beta \ddot{u}_{j+1} h_j^2 \tag{2.49}$$

$$\dot{u}_{j+1} = \dot{u}_j^* + \gamma \ddot{u}_{j+1} h_j, \tag{2.50}$$

where

$$u_j^* = u_j + \dot{u}_j h_j + \left(\frac{1}{2} - \beta\right) \ddot{u}_j h_j^2 \tag{2.51}$$

$$\dot{u}_j^* = \dot{u}_j + (1 - \gamma)\ddot{u}_j h_j \tag{2.52}$$

$$h_j = t_{j+1} - t_j, \tag{2.53}$$

and

$$\beta \in [0, 1/2], \ \ \gamma \in [0, 1]. \tag{2.54}$$

We obtain $\ddot{u}_{j+1}$ by solving

$$f(\ddot{u}_{j+1}, \dot{u}_j^* + \gamma \ddot{u}_{j+1} h_j, u_j^* + \beta \ddot{u}_{j+1} h_j^2, t_{j+1}) = 0. \tag{2.55}$$

The optimal parameters, and the ones we use in our results, are $\beta = 1/4$, $\gamma = 1/2$. In this case we have stability for any step size h, and, under mild regularity conditions, an order of convergence of 2 in time.

Our aim is to numerically solve

$$\mu \frac{\partial^2 w}{\partial t^2} + EI \frac{\partial^4 w}{\partial x^4} = q, \tag{2.56}$$

which can be translated into a problem of the type

$$M\ddot{u}(t) + Su(t) = p(t), \tag{2.57}$$

and therefore

$$f(\ddot{u}(t), \dot{u}(t), u(t), t) = M\ddot{u}(t) + Su(t) - p(t) = 0. \tag{2.58}$$

In the case of no load ($p(t) = 0$), the Newmark Method also satisfies the conservation of energy. [9]

For the Python implementation, we refer to attachment A.

2.6 The dynamic beam equation: Eigenvalue method

In case where there are no external forces and moments and we have homogeneous boundary conditions, the dynamic beam equation 2.26 can also be solved numerically with the eigenvalue method. The exact procedure is described in [10]. This report contains a short summary including the most important equations.

Let us rewrite system 2.46 or 2.47 as

$$M_e \ddot{y}(t) + S_e y(t) = 0, \tag{2.59}$$

where

$$y(t) = y_{\text{cantilever}}(t) = \begin{bmatrix} w(t) & Q_0(t) & M_0(t) \end{bmatrix}^\mathsf{T} \tag{2.60}$$

or

$$y(t) = y_{\text{two sided support}}(t) = \begin{bmatrix} w(t) & Q_0(t) & Q_L(t) \end{bmatrix}^\mathsf{T}, \tag{2.61}$$

and define $A = S_e^{-1} M_e \in \mathbb{R}^{N+2,N+2}$.

As before, in the eigenvalue method we look for solutions to the dynamic beam equation that consist of a time- and a space-dependent part,

$$y(t) = \sigma(t) \begin{bmatrix} w_k \\ \mu_k \end{bmatrix},$$

where $\begin{bmatrix} w_k \\ \mu_k \end{bmatrix}$ describes a space-dependent standing wave. These eigenvectors are determined by the eigenvalue equation

$$A \begin{bmatrix} w_k \\ \mu_k \end{bmatrix} = \lambda_k \begin{bmatrix} w_k \\ \mu_k \end{bmatrix}. \tag{2.62}$$

Following the derivation in [10], we find $N-2$ linearly independent eigenvectors $\begin{bmatrix} w_k \\ \mu_k \end{bmatrix}$ and time-dependent oscillations $\sigma(t)$, such that the solutions can be written as the linear combination

$$\begin{bmatrix} w(t) \\ \mu(t) \end{bmatrix} = \sum_{k=1}^{N-2} \left(\alpha_k \cos(\omega_k t) + \frac{\beta_k}{\omega_k} \sin(\omega_k t) \right) \begin{bmatrix} w_k \\ \mu_k \end{bmatrix} \tag{2.63}$$

with eigenfrequencies $\omega_k = \sqrt{\frac{1}{\lambda_k}}$, and coefficients

$$\alpha_k = \frac{w_k^\mathsf{T} M w(0)}{w_k^\mathsf{T} M w_k}, \qquad \beta_k = \frac{w_k^\mathsf{T} M \dot{w}(0)}{w_k^\mathsf{T} M w_k},$$

that depend on the initial conditions.

In the Python implementation, the eigenequation 2.62 is solved using the *eigs* function from the Scipy sparse package [11], see also attachment A.

3 Results and discussion

3.1 Static

In this section, the results from the performed simulations in the static case, Eq. (2.27), are presented. Two simulations were performed, corresponding to the two cases presented in the subsections 2.2.1 and 2.2.2, the former corresponding to the cantilever beam for three different parameter configurations and the latter corresponding the the beam supported at both ends, also with three different parameter configurations. In the figures, the different parameter configurations are represented as rows, and in the columns the solution and the derivative solution are presented. The case from subsection 2.2.1 is presented in Figure 3.1. The case from subsection 2.2.2 is presented in Figure 3.2.

From the figures, we see that the numerical solution using the finite element method corresponds very well to the analytical solution. The results for both the solution and the derivative are physically realistic. Since every parameter involved was tested for non-zero values, we conclude the general solution to be satisfactory in both the cantilever case as well as the case with two-sided support.

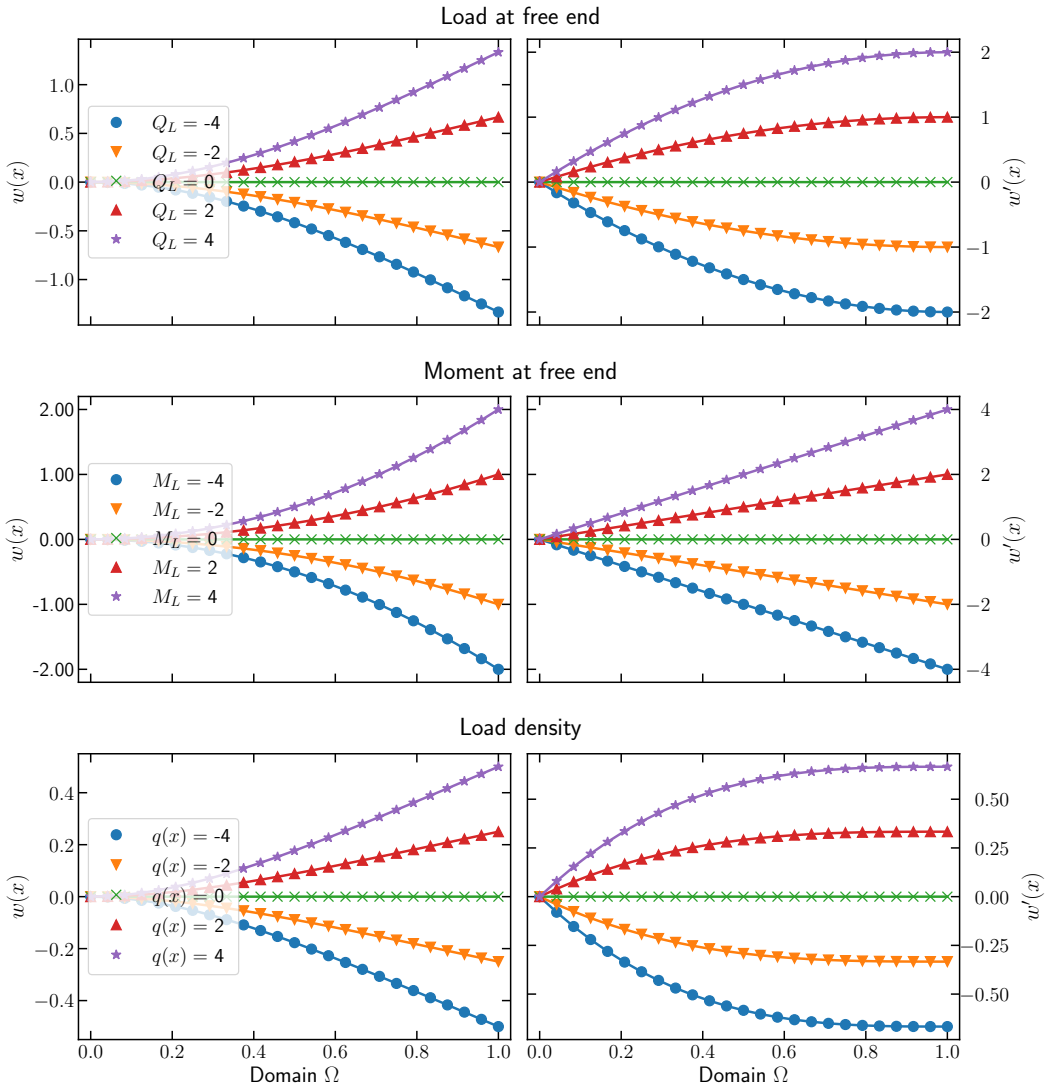

Figure 3.1: Parameter dependence of the static solution of the cantilever beam. The markers indicate the FEM numerical solutions, and the lines indicate the analytical solutions for the same parameters. Parameters used: $L, E, I = 1$, $N = 25$ grid points and the unspecified parameters are set to 0.

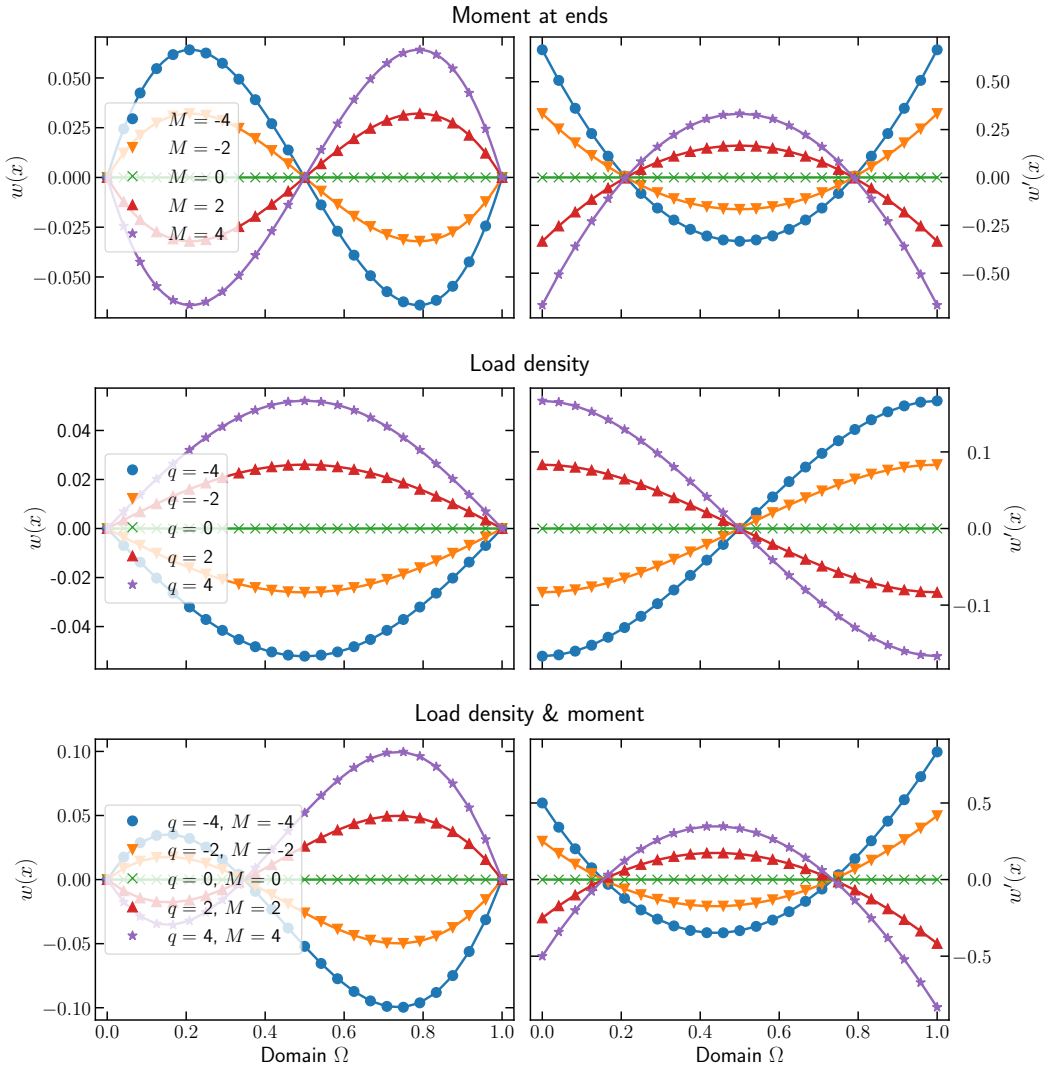

Figure 3.2: Parameter dependence of the static solution for the support at both ends ($w(0) = w(L) = 0$). The markers indicate the FEM numerical solutions, and the lines indicate the analytical solutions for the same parameters. Parameters used: $L, E, I = 1$, $N = 25$ grid points and the unspecified parameters are set to 0.

3.2 Dynamic

In chapter 2, two different methods for solving the time-dependent beam equation (2.59) were presented. In this section, we present the numerical experiments that were performed corresponding to the two methods.

3.2.1 Newmark method

We choose as the initial conditions for our solution $\dot{u}(t = 0)$, $u(t = 0)$ the solution of the static problem for some given parameters, and we initialize $\ddot{u}(t = 0) = 0$. Because of this, we observe that the system oscillates between two static solutions.

In the case of the beam being supported at both ends, we impose as the initial conditions the static solution correspondent to the parameters $\{M_L, M_0, a_0, a_L, q_0\}$ and let the system evolve with the parameters $\{M_L, M_0, a_0, a_L, q\}$, thus only changing the load parameter q. The Newmark Method is more general and allows for a different configuration, but in this manner we impose smooth initial conditions, and correspond to a realistic study case in which we suddenly apply a different load to a beam in equilibrium.

An animation of the oscillating beam solution is attached to this report as attachment B.

For further analysis, we consider the energy in the system. We start by considering the dynamic equation

$$M\ddot{u}(t) + Su(t) = p(t) \tag{3.1}$$

and defining the energy E as

$$E(t) = \frac{1}{2}\left(\dot{u}(t)^T M\dot{u}(t) + u(t)^T Su(t)\right). \tag{3.2}$$

we have that

$$\dot{E}(t) = \frac{1}{2}\dot{u}(t)^T\left(M\ddot{u}(t) + Su(t)\right) + \frac{1}{2}\left(\ddot{u}(t)^T M + u(t)^T S\right)\dot{u}(t). \tag{3.3}$$

In the case of symmetric matrices M, S,

$$\dot{E}(t) = \dot{u}(t)^T p(t). \tag{3.4}$$

Defining the external energy E_{ext} as

$$E_{ext}(t) = u(t)^T p(t) \tag{3.5}$$

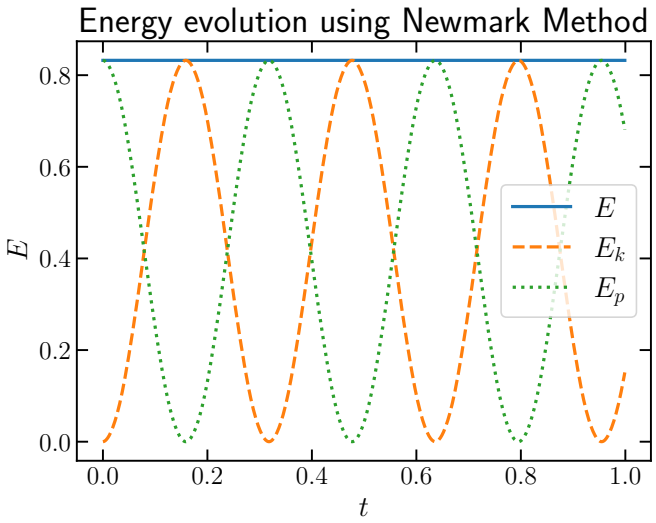

Figure 3.3: Evolution of the energy values using the Newmark Method, for a beam supported at both ends, initialized with zero acceleration as the solution of the static equation with parameters $\{M_0 = 0,\ M_L = 0\ a_0 = 0,\ a_L = 0,\ q = 10\}$ and evolving the system with the parameters $\{M_0 = 0,\ M_L = 0\ a_0 = 0,\ a_L = 0,\ q = 0\}$, with a constant time discretization parameter $h = 0.001$.

then, for a stationary load vector $\dot{p}(t) = 0$, we have that $E(t) = E_{ext}(t) + c$, where c is a constant in $\mathbb{R}$. Thus the energy should be conserved when $p(t) = 0$. It can be shown theoretically that the Newmark Method indeed conserves the energy quantity $E(t)$, as opposed to other methods. [9]

We can define the equivalent of potential and kinetic energy of a beam as

$$E_K = \frac{1}{2}\dot{u}(t)^T M \dot{u}(t) \tag{3.6}$$

and

$$E_p = \frac{1}{2}u(t)^T S u(t) \tag{3.7}$$

$$\tag{3.8}$$

and consider the total energy $E = E_k + E_p$.

We observe that, if we have load $q = 0$, the kinetic and potential energies oscillate, but its sum E remains approximately constant (Figure 3.3). In the case of having non-zero load, the energy E no longer remains constant, but it is equivalent to E_{ext}, (Figure 3.4).

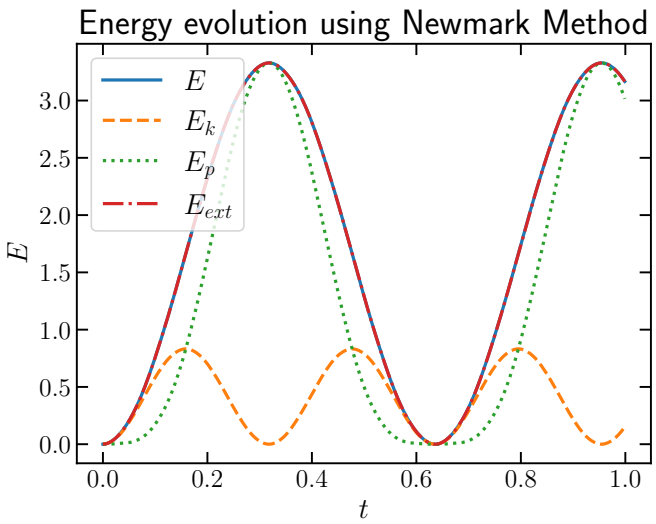

Figure 3.4: Evolution of the energy values using the Newmark Method, for a beam supported at both ends, initialized with zero acceleration as the solution of the static equation with parameters $\{M_0 = 0,\ M_L = 0\ a_0 = 0,\ a_L = 0,\ q = 0\}$ and evolving the system with the parameters $\{M_0 = 0,\ M_L = 0\ a_0 = 0,\ a_L = 0,\ q = 10\}$, with a constant time discretization parameter $h = 0.001$.

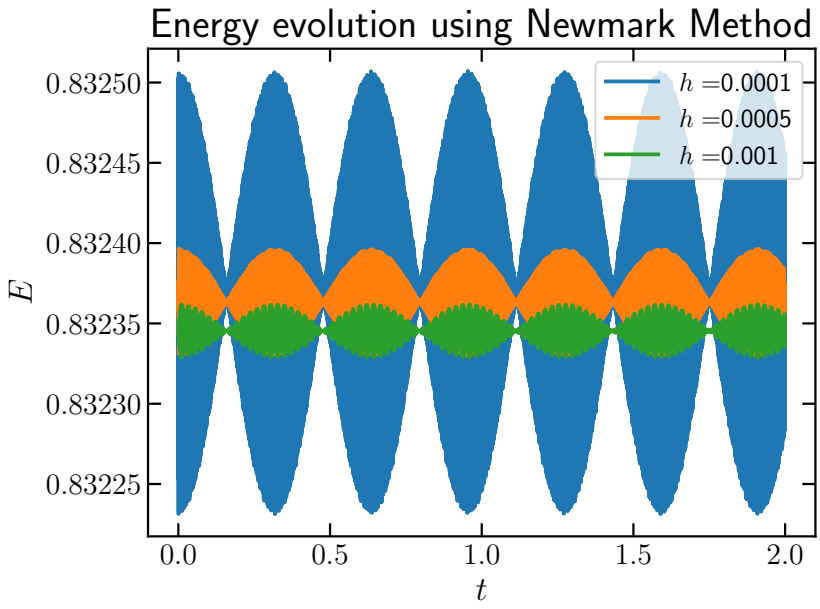

Figure 3.5: Evolution of the energy E using the Newmark Method, for a beam supported at both ends, initialized with zero acceleration as the solution of the static equation with parameters $\{M_0 = 0, M_L = 0\, a_0 = 0, a_L = 0, q = 10\}$ and evolving the system with the parameters $\{M_0 = 0, M_L = 0\, a_0 = 0, a_L = 0, q = 0\}$ and different time discretization parameters h. The total energy E oscillates and is modulated by an envelope wave.

However, looking more closely it is observed that the energy E does not remain constant but it oscillates. The behaviour of the energy is modulated by a wave with an envelope, see figure 3.5.
The mean energy $\langle E \rangle$ depends on the choice of the discretization parameter h, and the amplitude of the envelope wave increases as h decreases.

The dependency is non-polynomial, as observed in figure 3.6. The fact that it increases as h decreases can indicate a relation of this oscillations with floating-point errors. No further analysis of this phenomenon is presented here, but we refer to [12] for a more detailed discussion on energy fluctuation for Newmark method schemes.

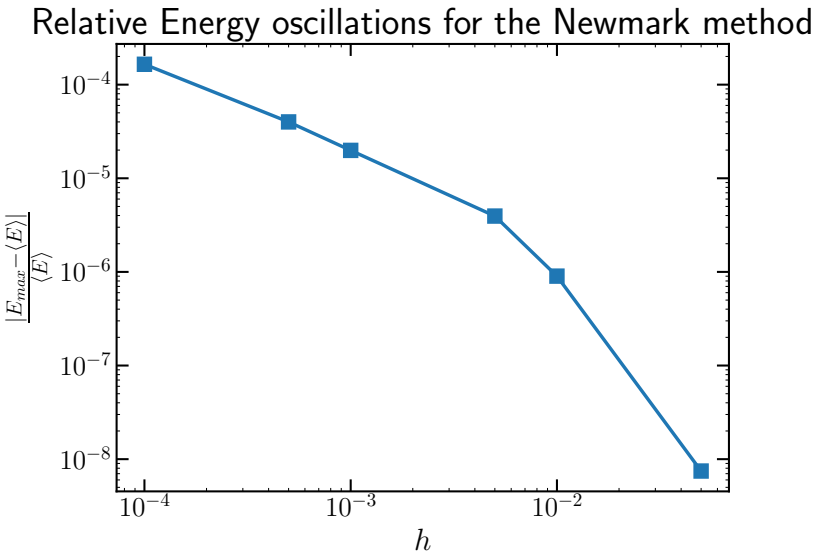

Figure 3.6: Dependency of the relative energy error with respect to the time discretization parameter h using the Newmark Method, or a beam supported at both ends, initialized with zero acceleration as the solution of the static equation with parameters $\{M_0 = 0,\ M_L = 0\ a_0 = 0,\ a_L = 0,\ q = 10\}$ and evolving the system with the parameters $\{M_0 = 0,\ M_L = 0\ a_0 = 0,\ a_L = 0,\ q = 0\}$.

3.2.2 Eigenvalue method

In this section we present the result of the following simulation experiments: comparison between numerical and analytical eigenfrequencies, visualization of a few of the first vibration modes for both the cantilever case and for the case with support at both ends, and finally an animation of these vibration modes with respect to time. The latter is attached to this report as attachment B.

The comparison between the numerical and analytical eigenfrequencies is plotted in Figure 3.7. For the numerical eigenvalue method, we took a system size of $N = 100$ eigenmodes. The numerical and analytical eigenfrequencies coincide up until around the 40th eigenvalue, after which they start diverging. This is explained by finite size effects - the analytical eigenvalue method forms a solution to the Euler-Bernoulli beam equation by a possibly infinite linear combination of eigenmodes. Because we allow for an infinte amount of eigenmodes, we build a solution within a complete function space. That is, every function can be reached. In the numerical eigenvalue method, we have only 100 eigenmodes available to build, or better, approximate the solution. These 100 eigenmodes do not form a complete space and therefore the higher frequencies try to compensate for missing eigenmodes, explaining the difference between numerical and analytical eigenfrequencies for high j.

The vibration eigenmodes resulting from the numerical eigenvalue method are illustrated in Figure 3.8. Their shapes coincide with their analytical counterparts up until mode five, which was the maximum amount of modes we included in this experiment, mainly for visual reasons. Attachment B gives an animation of the vibrating eigenmodes that were found numerically.

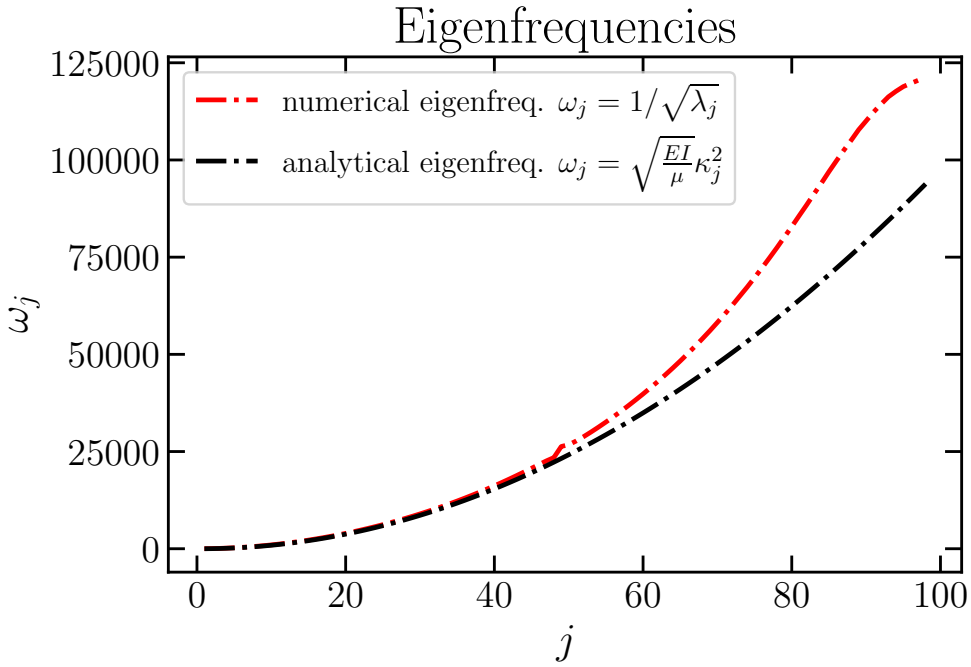

Figure 3.7: Comparison between numerical and analytical eigenfrequencies. For small j, they coincide perfectly. For high j, the difference is explained by finite-size effects.

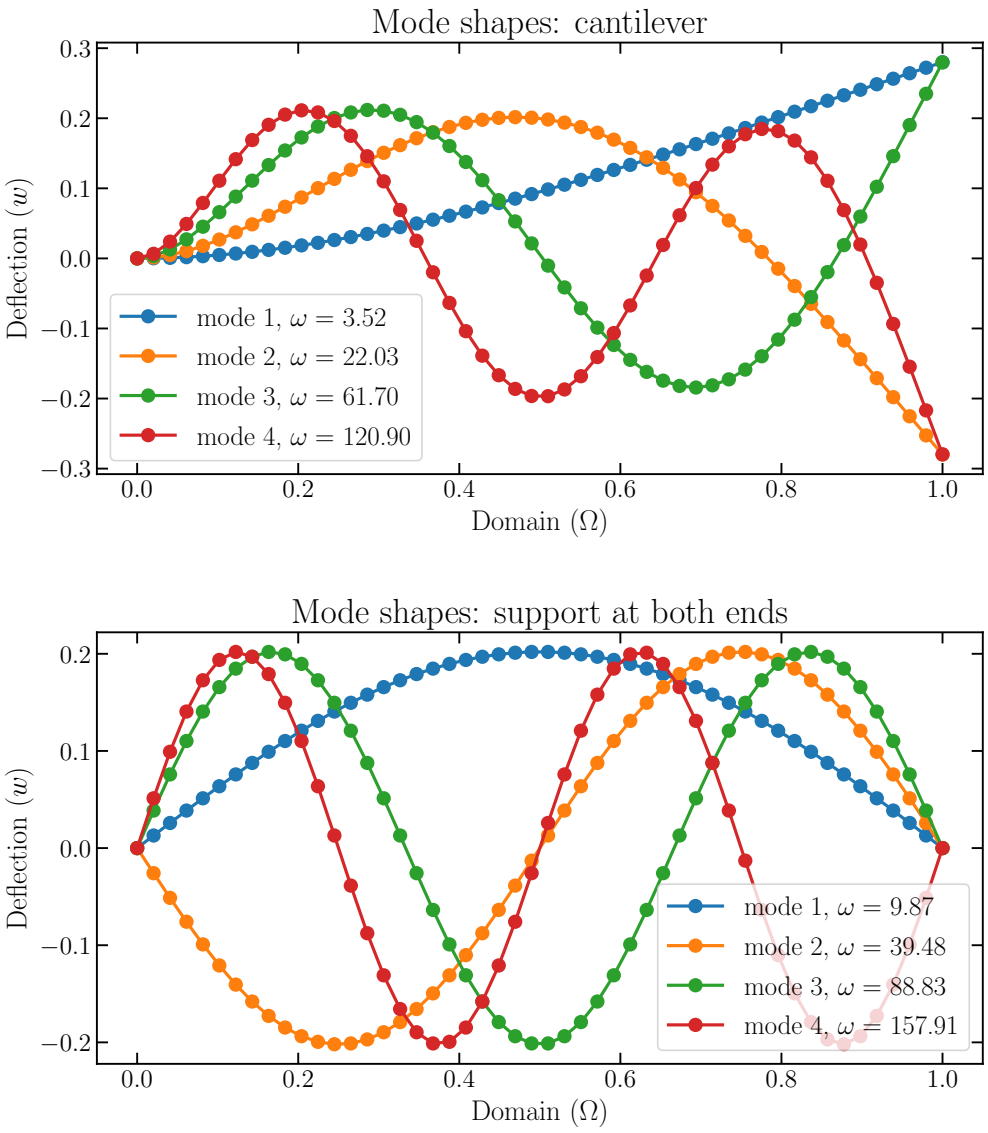

Figure 3.8: First five vibration modes for the cantilever (top) and support at both ends (bottom) cases, resulting from the numerical eigenvalue method. They coincide perfectly with their analytical counterparts.

4 Conclusion

The numerical simulations that were performed for the static case showed good results that are in perfect agreement with analytical solutions. Note however, that only constant load densities were tested, and there may be applications where a non-constant density function might be of interest. This is already implemented, but the full analysis could serve as a continuation of the project presented here.

The dynamic problem was solved using two different methods: the Newmark method and the eigenvalue method. For the Newmark method, we obtain good and realistic solutions, but looking more closely, undesired energy fluctuations are observed. They increase as the time discretization parameter h decreases. This oscillations are however periodic, and energy is conserved over large time windows, as opposed to other methods in which numerical damping occurs. The method is therefore considered successful, and the relative energy error (the amplitude of the energy oscillations divided by the mean energy) due to the oscillations is at most 0.015% for $h = 0.0001$, and therefore considered negligible.

Using eigenvalue analysis, we were able to make a realistic simulation of the dynamic solution to the beam equation. The drawback of this method is that it requires a certain (and very basic) parameter setup. The advantage, compared to the Newmark method, is that it is less costly in terms of computational power. Moreover, it gives more insight into beam vibrations and the underlying eigenfrequencies.

For future studies, it would be interesting to perform a more thorough error analysis for both the Newmark and the eigenvalue method. This could also be interesting from a performance perspective. Moreover, one could look into under what exact conditions these mathematical results are applicable in real-life situations.

Bibliography

[1] O. Morgul, "Dynamic boundary control of a Euler-Bernoulli beam," *IEEE Transactions on Automatic Control*, vol. 37, no. 5, pp. 639–642, 1992.

[2] J. Yang, L. Jiang, and D. Chen, "Dynamic modelling and control of a rotating Euler–Bernoulli beam," *Journal of Sound and Vibration*, vol. 274, no. 3, pp. 863–875, 2004.

[3] S. Choura, S. Jayasuriya, and M. A. Medick, "On the Modeling, and Open-Loop Control of a Rotating Thin Flexible Beam," *Journal of Dynamic Systems, Measurement, and Control*, vol. 113, pp. 26–33, 03 1991.

[4] Y. Shi, W. Guo, and C. Ru, "Relevance of Timoshenko-beam model to microtubules of low shear modulus," *Physica E: Low-dimensional Systems and Nanostructures*, vol. 41, no. 2, pp. 213–219, 2008.

[5] Ömer Civalek and Çiğdem Demir, "Bending analysis of microtubules using nonlocal Euler–Bernoulli beam theory," *Applied Mathematical Modelling*, vol. 35, no. 5, pp. 2053–2067, 2011.

[6] W. Bottega, *Engineering Vibrations*. CRC Press, 2014.

[7] M. Karow, "Script 1 - Bending of Bernoulli beams and FEM," 2012.

[8] M. Karow, "Script 3a - Vibrations of a uniform Bernoulli beam," 2021.

[9] M. Karow, "Script 2 - The Newmark Method," 2016.

[10] M. Karow, "Script 3b - The eigenvalue method for undamped vibrations," 2021.

[11] P. Virtanen *et al.*, "SciPy 1.0: Fundamental Algorithms for Scientific Computing in Python," *Nature Methods*, vol. 17, pp. 261–272, 2020.

[12] S. Krenk, "Energy conservation in Newmark based time integration algorithms," *Computer Methods in Applied Mechanics and Engineering*, vol. 195, no. 44-47, pp. 6110–6124, 2006.

Attachments to the report

A. Code
B. Videos of numerical solutions